Infrared Detection Using Transparent and Flexible Field-Effect Transistor Array with Solution Processable Nanocomposite Channel of Reduced Graphene Oxide and P(VDF-TrFE)

*Tran Quang Trung, Subramaniyan Ramasundaram, and Nae-Eung Lee**

Photodetectors using optically responsive graphene (Gr) or reduced graphene oxide (R-GO) on rigid substrates have showed promising results for detection of broad band light including infrared (IR). However, there have been only a few reports on Gr or R-GO photodetectors with new functionalities such as optical transparency and/or flexibility. Herein, a new kind of transparent and flexible IR photodetector is presented using a field-effect transistor (FET) structure in which an IR-responsive nanocomposite layer of R-GO and poly(vinylidenefluoride-co-trifluoroethylene) (P(VDF-TrFE)) is employed as the channel. The IR photodetector exhibits high IR responsivity, stability, and reproducibility under mechanical strain and ambient conditions. In addition, the capability of measuring the distribution of responses from each device in the transparent and flexible nanocomposite FET array under IR radiation from the human body is also demonstrated. Therefore, the development of a flexible IR photodetector with high responsivity, transparency, ease of integration, and stability in an ambient environment is a suitable alternative approach for achieving the stable monitoring of IR in many flexible and transparent electronic systems.

1. Introduction

The development of mechanically flexible and optically transparent electronic devices that are light-weight, unbreakable, transparent, and flexible, for the next generation of optoelectronic devices, has attracted tremendous research efforts due to their potential to cause significant commercial impact in a wide variety of areas.[1–8] In the field of optoelectronic devices, photodetection in the infrared (IR) region can be utilized in an extensive range of applications including telecommunication, thermal imaging, and remote sensing.[3,9–14] Additionally, increasingly unique applications in various new areas, such as military detection, biomedical temperature monitoring, and portable devices, have recently become the focus of current research.[1,2,12] Furthermore, developing a flexible photodetector that requires transparency, flexibility, lightweight, and mechanical shock-resistive sensing elements is interesting in the field of civil engineering.[2] Therefore, the development of a new IR detector with high responsivity, transparency, ease of integration, and stability in an ambient environment is a suitable alternative approach for realizing the stable monitoring of IR in many flexible and transparent electronic systems.

Graphene (Gr) has remarkable optical properties for photodetection.[15,16] It has gapless energy dispersion and strong inter band transition, which help Gr absorb photons over a wide range of wavelengths (from the visible to terahertz range).[12,15–17] Based on these features, Gr photodetectors using field-effect transistor (FET),[9,12,18–27] and photoresistor[3,28] structures have been successfully fabricated and used as terahertz, IR, visible, and UV light detectors. The sensing mechanism of Gr photodetectors contains three main mechanisms (photovoltaic, photothermalelectronic, and bolometric effects)[12,29] that depend on the device design, wavelength range, and the materials that are used.

In recent reports, IR detectors based on Gr have been demonstrated to be highly responsive to IR due to the generation of internal electric fields at the electrodes/Gr interfaces where charge transfer between the electrode and Gr leads to band bending and as a result photogenerated carriers are separated by Schottky barrier modulation (i.e., internal electric fields).[24–27] The absence of a strong electric field in the Gr sheet, where most of the electron–hole pairs are generated are recombined

Dr. T. Q. Trung
School of Advanced Materials Science & Engineering
Sungkyunkwan University (SKKU)
Suwon, Kyunggi 440–746, South Korea
Dr. S. Ramasundaram
Center for Water Resource Cycle Research
Korea Institute of Science and Technology
Hwarangno 14 gil, Seongbuk-gu, Seoul 136–791, South Korea
Prof. N.-E. Lee
School of Advanced Materials Science & Engineering
SKKU Advanced Institute of Nanotechnology (SAINT)
and Samsung Advanced Institute for Health
Sciences & Technology (SAIHST)
Sungkyunkwan University (SKKU)
Suwon, Kyunggi 440–746, South Korea
E-mail: nelee@skku.edu

DOI: 10.1002/adfm.201404582

without any contribution to the external photocurrent.[24] Because of these features of Gr IR detectors, the light source must be focused adjacently to the electrodes/Gr for generation of photocurrent. This is inconvenient for real-life applications. In addition, there have been recent reports on IR detectors based on reduced graphene oxide (R-GO), which has a lower carrier mobility compared to Gr,[30,31] and bandgap is tuneable.[32] This feature of R-GO allows for photogenerated electron–hole pairs to be dissociated by an external voltage before they recombine. However, both single layer Gr and a few layers of R-GO have low light absorbance (≈2%–6.9% of normally incident light).[31] These materials also require the use of many processing steps such as transfer of CVD (chemical-vapour deposited) Gr, mechanical exfoliation of Gr,[33] and formation of a thin, continuous R-GO network[30,34,35] for integration into the IR sensor devices, which makes their fabrication complex, costly, of low yield, and difficult to control. It is reasonable to consider that developing IR sensing materials based on R-GO, which can be incorporated into FETs with a simple solution process, will reinforce the responsivity to IR and improve stability in ambient conditions.

Herein, we developed a new kind of transparent and flexible IR detector using an FET structure in which an IR-responsive nanocomposite layer of R-GO and poly(vinylidenefluoride-co-trifluorothylene) (P(VDF-TrFE)) was employed as the channel. The novelty of the R-GO/P(VDF-TrFE) nanocomposite FET IR sensor is found in the combination of inserting conductive and IR-responsive R-GO nanosheets into the hydrophobic copolymer (P(VDF-TrFE) matrix as an IR sensing layer, which can be easily coated onto a large-area substrate for the fabrication of transparent and flexible devices using a simple spin-coating method. Additionally, the total amount of R-GO in an R-GO/P(VDF-TrFE) nanocomposite can be controlled by adjusting the layer thickness or R-GO concentration in the R-GO/P(VDF-TrFE) nanocomposites for enhanced IR absorbance. Furthermore, the hydrophobic P(VDF-TrFE) matrix served to minimize environmental effects caused by polar solvents, moisture, and/or water vapour on the sensing capabilities in ambient conditions and also to enhance the IR absorbance of the nanocomposite. The IR response of the transparent and flexible nanocomposite FETs was examined under IR exposure with different intensities. The transparent and flexible R-GO/P(VDF-TrFE) nanocomposite FET presented higher IR responsivity than the R-GO channel FET. The IR responsivity of the transparent and flexible nanocomposite FET was also examined under mechanical strain. The IR sensor exhibited high IR responsivity, stability, and reproducibility under mechanical strain and ambient conditions. Finally, the ability to measure the response distribution of each device in a transparent and flexible nanocomposite FET array to IR radiation of the human body was also demonstrated.

2. Results and Discussion

The IR-responsive nanocomposite FETs were fabricated in a bottom-gate and bottom-contact configuration. The schematic of the FET structure is shown in **Figure 1**a. Using a simple solution-based fabrication process (spin-coating), a transparent and flexible array with 16 IR-responsive nanocomposite FETs was fabricated on a flexible and transparent polyethersulfone (PES) substrate (Figure 1c,d). The flexible nanocomposite FET array is transparent in visible light and has the ability to respond to IR radiation from the human body. Figure 1b shows the distribution of the normalized current ($(I_{DS} - I_{DS0})/I_{DS0} \times 100\%$) obtained from each device in the array when a finger was moved near to a quadrant of the device array.

The R-GO/P(VDF-TrFE) nanocomposite thin films, used as channels in the FET, were fabricated with varying thicknesses (200 and 250 nm) and R-GO concentrations (8, 10, and 12 wt%). The size and distribution of the R-GO nanosheets within the polymer matrix P(VDF-TrFE) of the nanocomposite thin film, with an R-GO concentration of 12 wt%, were confirmed by atomic force microscopy (AFM) and field-emission scanning electron microscopy (FE-SEM), respectively. For a more detailed discussion, see Figure S1a,b, Supporting Information. IR response characteristics of the nanocomposite FETs with varying R-GO concentrations (8, 10, and 12 wt%) were systematically measured. The responsivity of nanocomposite FET increases with the R-GO concentration increased (Figure S2, Supporting Information) but the optical transmittance was decreased (Figures S3, Supporting Information). For a high performance transparent nanocomposite FET for IR sensing, therefore, the optical transmittance and IR responsivity can be compromised by controlling the R-GO concentration.

To evaluate the fundamental properties of the nanocomposite FET, the devices were fabricated on both glass and flexible substrates. First, we fabricated the R-GO/P(VDF-TrFE) nanocomposite FET on a glass substrate to investigate its response to IR and compared the responsivities of the R-GO/P(VDF-TrFE) nanocomposite and R-GO FETs. It should be noted that the R-GO FET has a larger network of R-GO within the channel. To investigate the responsivity of the nanocomposite FET to IR under mechanical strain in order to demonstrate the potential for application in transparent flexible electronics, a transparent and flexible nanocomposite FET with mechanical flexibility, low weight, and ease of attachment was fabricated and investigated.

Response of the transparent nanocomposite FET to IR was investigated by irradiating the device surface with IR from a halogen lamp. A filter was placed in front of the halogen lamp to cut off all wavelengths shorter than 800 nm. **Figure 2**a shows the transfer characteristics of the device measured at various IR intensities (from 500 to 2000 mW cm^{-2}). The minimum drain current ($I_{DS,min}$: the currents were extracted at the charged neutrality point of the transfer characteristics) values of the transparent nanocomposite FETs with an R-GO concentration of 8 wt% and a thickness of 200 nm were measured at different source-drain voltages (V_{DS}) (9, 12, and, 15 V) and are presented as a function of IR intensity (P_{IR}) in Figure 2b. Figure 2c represents the IR response for one of the devices, where the response of the normalization current ($(I_{DS} - I_{DS0})/I_{DS0}$) to the IR response is plotted as a function of time (with different IR intensities).

The types of detectors employing conductive IR-responsive materials can be classified as either photosensors or thermal sensors.[12,29] Photosensors are based on the photovoltaic effect in which electron–hole pairs are generated by the absorption of

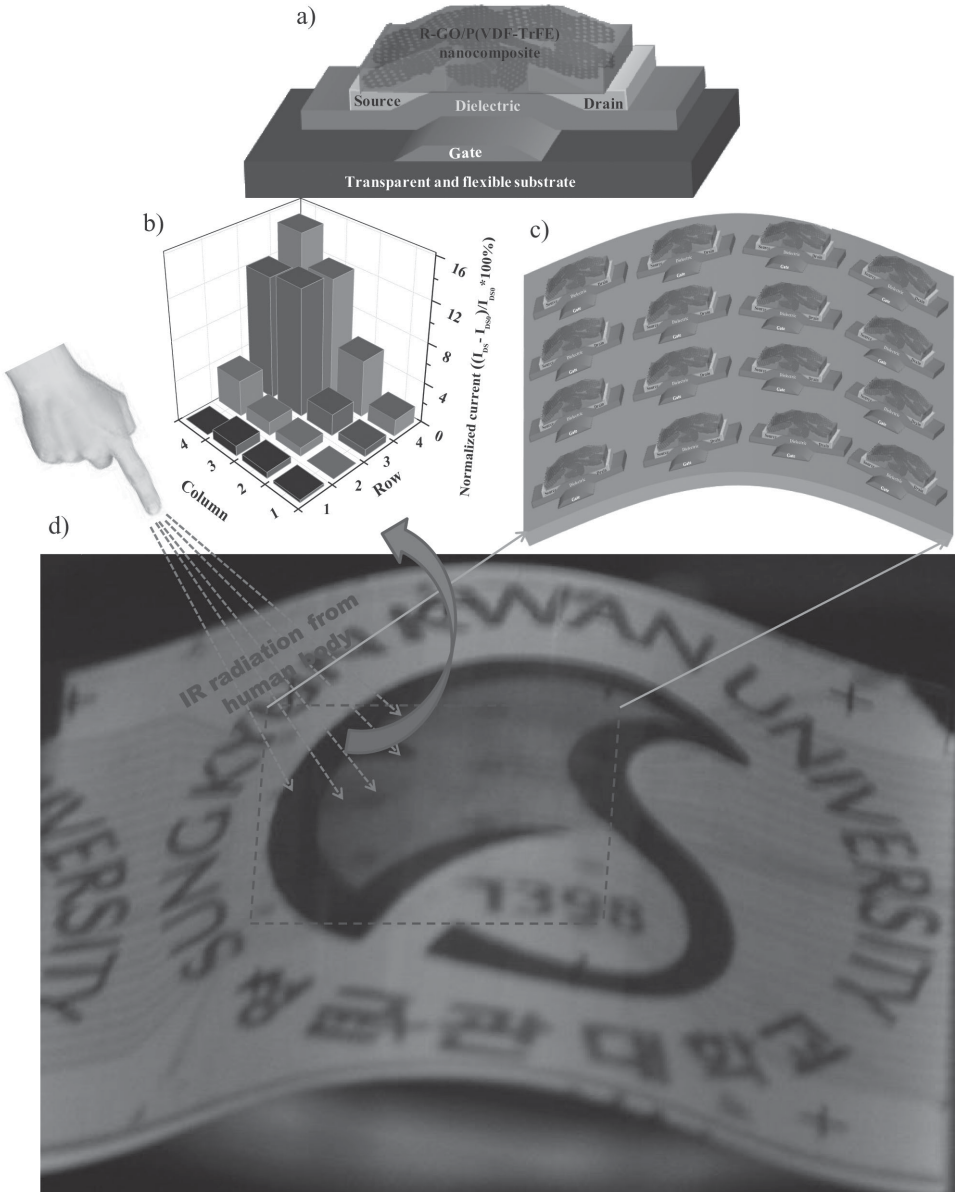

Figure 1. a) Schematic structure of the transparent and flexible FET with IR-responsive R-GO/P(VDF-TrFE) nanocomposite channel. b) The distribution of the normalized current $(I_{DS} - I_{DS0})/I_{DS0} \times 100\%$ obtained from each device in the array when a finger is moved close to the quadrant of the device array. c) Schematic structure of the device array. d) The image of the transparent and flexible nanocomposite FET array, which can respond to IR radiation from both an IR source and a human body, fabricated on a large area of a transparent and flexible polyethersulfone (PES) substrate (the logo and text on the paper behind the substrate are clearly visible).

photons. Alternatively, thermal sensors, such as a bolometric sensor, absorb heat which is transferred from IR source to the device via conduction, convection, or radiation and the heat induces a resistance change within the sensing material. In our IR detector that uses the R-GO/P(VDF-TrFE) nanocomposite, the R-GO filler in the P(VDF-TrFE) matrix is shown to absorb photons in the IR and heat from the IR source. Upon IR exposure, the R-GO filler can absorb photons and heat to produce electron–hole pairs and heat within the R-GO/P(VDF-TrFE) nanocomposite thin film, respectively, which produces a change in resistance. To demonstrate that the conductivity of channel is dependent on temperature, response of R-GO/P(VDF-TrFE) FET to temperature from room temperature (25 °C) to 45 °C with an interval temperature of 2 °C were measured. Figure S4a, Supporting Information, shows the transfer characteristics of the device measured at various temperatures. And, the $I_{DS,min}$ values extracted at the charge neutrality point of the transfer characteristics are presented as a function of temperature in Figure S4b, Supporting Information. The changes in the conductance of nanocomposite channel are affected by temperature variation, which implies that the heat transfer from IR source can also cause change of the conductance in R-GO/P(VDF-TrFE) nanocomposite channel. Therefore, it is presumed that the IR responsivity in the nanocomposite FET is attributed to a

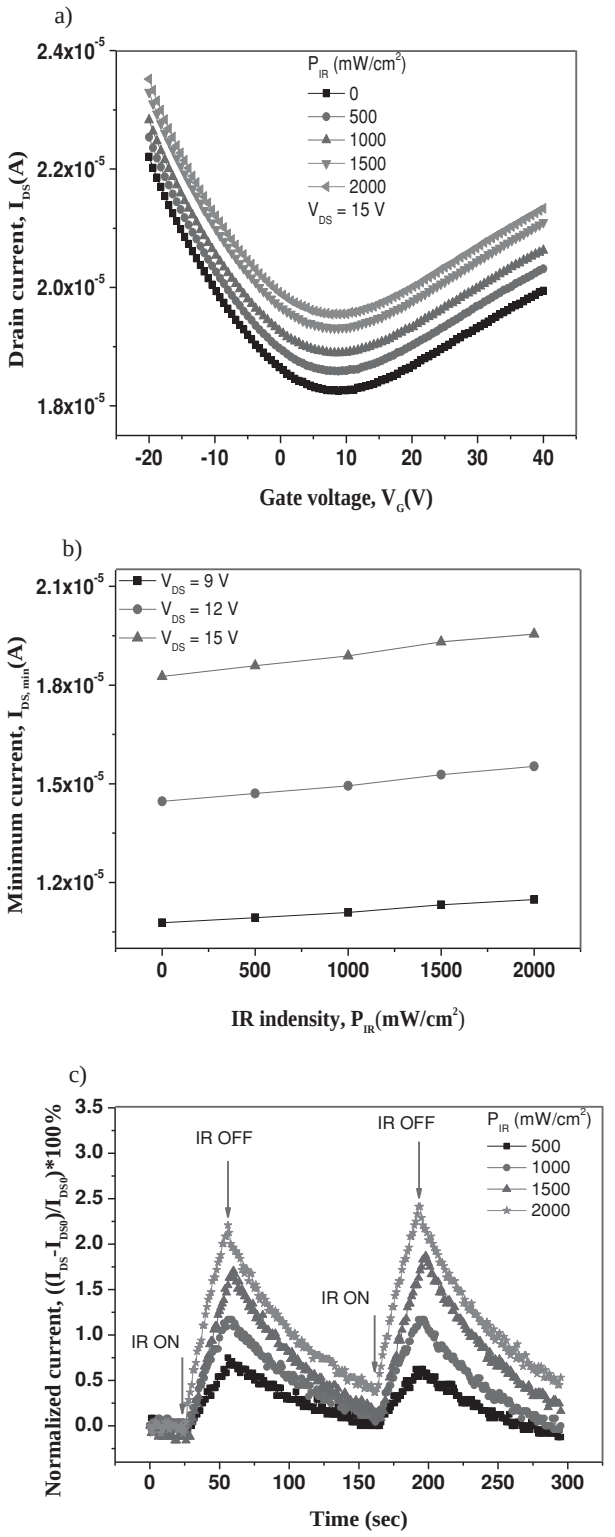

Figure 2. a) The transfer characteristics of the transparent FET with the nanocomposite channel (R-GO concentration of 8 wt% and thickness of 200 nm) under various IR intensities at V_{DS} = 15 V. b) The minimum current ($I_{DS,min}$) of the transparent nanocomposite FET as a function of P_{IR} at different source-drain voltages, V_{DS}. c) Time-dependence of normalized current, (I_{DS} – I_{DS0})/I_{DS0} × 100% (I_{DS}: current under IR exposure and I_{DS0}: current without IR exposure) under different IR intensities at V_{DS} = 9 V and V_G = 10 V.

combination of two possible mechanisms: the photovoltaic and bolometric effects.

To more clearly understand the IR responses of the transparent nanocomposite FET, we compared the same FET structures with the nanocomposite and networked R-GO channels. **Figure 3**a,b presents the $I_{DS,min}$ modulation and time-dependent responses of the R-GO FET and the transparent nanocomposite FET to IR exposure, respectively. The R-GO FET was exposed to IR with the P_{IR} from 500 to 2000 mW cm^{-2}. The slope of the $I_{DS,min}$ modulation (Figure 3a) and current response (Figure 3b) of the transparent nanocomposite FET are higher than those of the R-GO FET. From the data in Figure 3a, we can calculate the responsivities of devices to IR by using $R = \frac{(I_{DS,min} - I_{DSO,min})}{I_{DSO,min}} \times 100\%$. The responsivity of the R-GO FET and R-GO/P(VDF-TrFE) FET are $R_{R\text{-}GO\ FET}$ = 3.53%/W cm^{-2} and $R_{R\text{-}GO/P(VDF\text{-}TrFE)\ FET}$ = 7.12%/W cm^{-2}. We can see that the responsivity of the R-GO/P(VDF-TrFE)FET is higher than that of the R-GO FET by a factor of two. The enhancement of IR absorption in the R-GO/P(VDF-TrFE) nanocomposite presumably comes from the amount of R-GO and the thickness of nanocomposite film larger than those of the few layer R-GO networked film. Therefore, the absorption of IR radiation and heat from IR source within the nanocomposite can be higher. Thus, the IR responsivity is expected to be enhanced for an R-GO/P(VDF-TrFE) FET-based IR detector.

Interestingly, the transparent nanocomposite FET is also highly responsive to IR radiation from the human body. Figure 3c,d shows the response of the R-GO FET and transparent nanocomposite FET (with concentrations of 8 wt% and thicknesses of 200 nm) to IR radiation from a human finger. The nanocomposite FET had higher responsivity than the R-GO FET, which is primarily attributed to the higher absorption of the IR from a finger in the nanocomposite due to the larger amount of R-GO nanosheets in the nanocomposite and its larger thickness compared to the networked R-GO channel. In addition, the absorption of IR radiation from the human body may include absorption of IR by the P(VDF-TrFE) matrix in the nanocomposite. The IR absorption spectrum of P(VDF-TrFE) (Figure S5, Supporting Information) shows strong absorption peaks in the wavelength range from 6500 to 9500 nm and from 11 000 to 12 000 nm. According to thermal radiation theory (near human body temperature, 310 K), the wavelength emitted from the human body ranges from 3000 to 70 000 nm. Consequently, P(VDF-TrFE) is expected to efficiently absorb IR radiation from the human body. To elucidate the role of P(VDF-TrFE) in the nanocomposite film, a nanocomposite of polyurethane (PU) matrix was prepared. A FET based on R-GO/PU nanocomposite as a channel which has the same R-GO concentration and thickness as those of R-GO/P(VDF-TrFE) FET was fabricated and response of the device to IR radiation from human body was investigated. The response signal of R-GO/PU FET is lower than that of R-GO/P(VDF-TrFE) but still higher than that of R-GO FET (see Figure S6, Supporting Information). The results are primarily attributed to the higher absorption of IR radiation from the human body by the P(VDF-TrFE) than PU matrix in the nanocomposite. The P(VDF-TrFE) layer shows

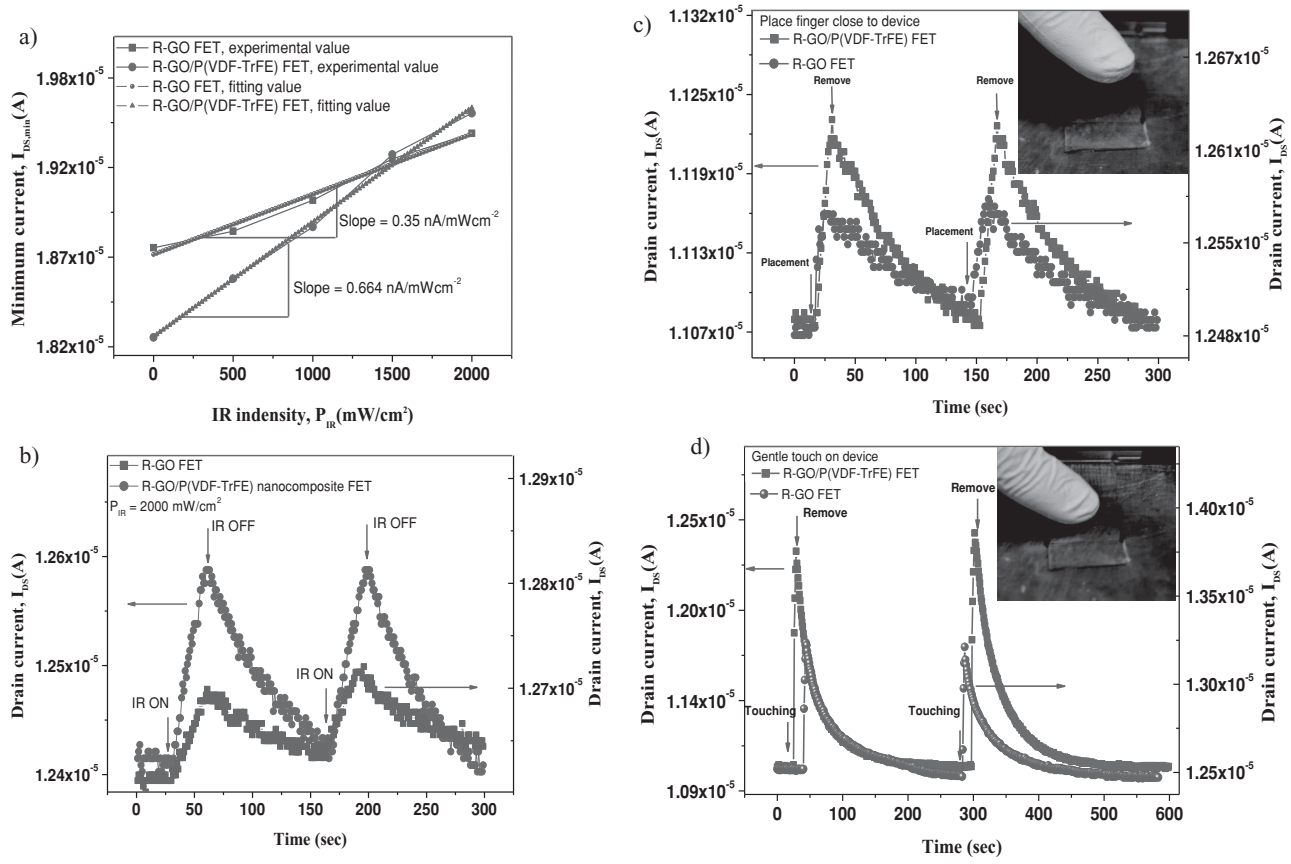

Figure 3. Comparing the responsivity of the R-GO/P(VDF-TrFE) nanocomposite FET and the R-GO FET to IR light and IR from a human body. a) The $I_{DS,min}$ of the transparent nanocomposite FET and R-GO FET were plotted as a function of P_{IR} at V_{DS} = 15 V. b) Time-dependence of I_{DS} under a P_{IR} of 2000 mW cm^{-2} of the nanocomposite FET and R-GO FET at V_{DS} = 9 V and V_G = 10 V. Time-dependence of I_{DS} in the nanocomposite FET and R-GO FET with a finger placed near the device c), and with a finger gently touching the device d) at V_{DS} = 9 V and V_G = 10 V.

strong absorption peaks in the wavelength range from 6500 to 9500 nm and from 11 000 to 12 000 nm, whereas the PU shows only one absorption peak at 9000 nm (Figure S5, Supporting Information). Because of the larger amount of R-GO nanosheets in the R-GO/PU nanocomposite and its larger thickness than the networked R-GO channel, the response signal of R-GO/PU is still higher than that of R-GO FET.

To investigate the response behaviour of the R-GO/P(VDF-TrFE) nanocomposite IR detector under mechanical strain, transparent and flexible R-GO/P(VDF-TrFE) nanocomposite FETs that are light weight and easily attached to an object were fabricated on PES substrates. Figure S7a, Supporting Information, presents the ambipolar transfer characteristics of transparent and flexible nanocomposite R-GO FETs with a concentration of 12 wt% and a thickness of 250 nm. The electron and hole field-effect mobilities of these FETs were lower than those of the nanocomposite device on a glass substrate. These results are attributed to the differences in the thickness and materials of the gate dielectric layers employed in the devices on the flexible and glass substrates. A more detailed discussion of this phenomenon has been presented in previously.[36] To confirm the optical transmittance of the transparent and flexible devices, total optical transmission spectra were measured through the stacked blanket layers on a PES substrate that had the same thickness as the layers in the transparent and flexible nanocomposite FET structure. As shown in Figure S7b, Supporting Information, the optical transmission of the PES substrate with stacked blanket layers in the visible wavelength (ranging from 350 to 800 nm) was about 55%. The optical images of the transparent and flexible nanocomposite FETs (see the inset in Figure 7b, Supporting Information) show the degree of optical transparency: text on paper placed directly behind the devices is clearly visible.

To study the electrical behaviours of the transparent and flexible nanocomposite FETs in response to IR under mechanical strain, the transfer characteristics of devices were measured under simultaneous IR exposure and straining. The typical responses of the drain current (I_{DS}) are plotted in **Figure 4**a–c. The $I_{DS,min}$ values extracted from transfer characteristics at V_{DS} = 9 V in Figure 4a–c are presented as a function of P_{IR} in Figure 4d. The response behaviours of the transparent and flexible devices to IR under tensile and compressive strains showed the same tendencies as those of the flexible device without strain. The modulation of the I_{DS} in the transparent and flexible nanocomposite FET under tensile and compressive strains (Figure 4d) can be understood by examining the

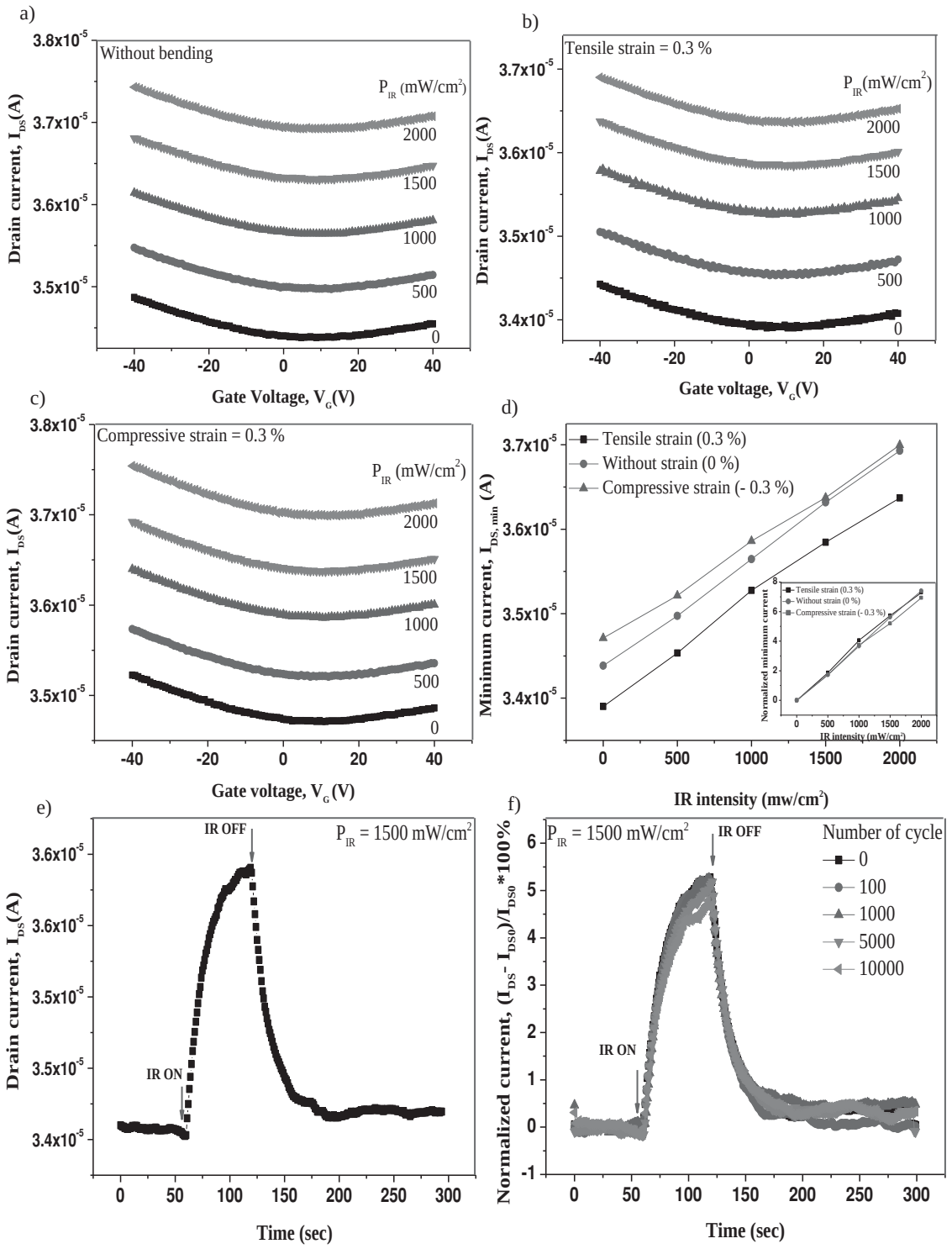

Figure 4. The transfer characteristics of the transparent and flexible R-GO/P(VDF-TrFE) nanocomposite FET under various P_{IR} at V_{DS} = 9 V: a) without bending, b) under tensile strain, and c) under compressive strain. d) The $I_{DS,min}$ was extracted from the transfer characteristics as a function of P_{IR} under mechanical strain and without mechanical strain at V_{DS} = 9 V. The insert in the figure shows the normalized minimum current, $((I_{DS,min} - I_{DS0,min})/I_{DS0,min}) \times 100\%$ ($I_{DS,min}$: minimum current under IR exposure and $I_{DS0,min}$: minimum current without IR exposure), as a function of P_{IR} under mechanical strain and without mechanical strain. e) Time-dependence of the I_{DS} under a P_{IR} of 1500 mW cm^{-2} for the transparent and flexible R-GO/P(VDF-TrFE) nanocomposite FET before cyclic bending at V_{DS} = 9 V and V_G = 10 V. f) Time-dependencies of the normalized current, $((I_{DS} - I_{DS0})/I_{DS0}) \times 100\%$, upon IR exposure with a P_{IR} of 1500 mW cm^{-2} at V_{DS} = 9 V and V_G = 10 V after the device was cyclically bent for 100, 1000, 5000, and 10 000 bending cycles at a tensile strain of 0.3%.

change of the resistance in the R-GO/P(VDF-TrFE) nanocomposite channel. It is known that in nanocomposite materials, the electrical transport mechanism is governed by the distribution of the filler material in the matrix polymer. Here, the filler R-GO nanosheets in the P(VDF-TrFE) matrix were demonstrated to have a larger contact area between neighbouring R-GO nanosheets compared to the end-to-end connections (see Figure S1, Supporting Information). Therefore, the electrical conduction mechanisms of the R-GO/P(VDF-TrFE) nanocomposite thin film can be described by tunnelling through R-GO nanosheet junctions and hopping between the R-GO nanosheets (coupling at R-GO nanosheet junctions), which may be expected to change upon an applied strain. Tensile strain may reduce coupling at nanosheet junctions, leading to an increase of the resistance of the R-GO/P(VDF-TrFE) nanocomposite film, thereby decreasing the I_{DS} (Figure 4 and Figure S8, Supporting Information). Conversely, the I_{DS} increased as the compressive strain increased (Figure 4d and Figure S9, Supporting Information), which results from the decrease of resistance in the R-GO/P(VDF-TrFE) nanocomposite channel, presumably due to reinforcement of coupling at the nanosheet junctions under compressive strain.

For more clarity, using the data in Figure 4d, the normalized minimum current $\left(\frac{I_{DS,min} - I_{DSO,min}}{I_{DSO,min}} \times 100\%\right)$ was plotted as a function of P_{IR} (the insert in Figure 4d). We can see that the responsivity of the device to IR both under strain and without strain was essentially unchanged. Even though the drain current is affected by the strain, normalizing the responses can provide strain-independent detection of IR.

To further investigate the IR sensing performance of the transparent and flexible R-GO/P(VDF-TrFE) nanocomposite FET, the sensing characteristics were studied by measuring the time-dependent I_{DS} under simultaneous IR radiation and an applied strain. Figure 4e shows the time-dependence of the I_{DS} under IR exposure only. Conversely, Figure S10a,b, Supporting Information, shows the time-dependence of I_{DS} under tensile straining followed by IR exposure and compressive straining followed by IR exposure, respectively. The results in Figure 4e and Figure S10a,b, Supporting Information, indicate that the IR sensing behaviour of the transparent and flexible nanocomposite FET under IR exposure and the device exposed to simultaneous strain and IR exposure are the same. This means that the IR sensing mechanism of the device is not affected by mechanical strain.

In addition, to evaluate the reliability of the transparent and flexible R-GO/P(VDF-TrFE) nanocomposite FETs after repetitive mechanical deformations, the sensing capability of the device was evaluated after cyclic bending of the devices. The IR response of devices subjected to 100, 1000, 5000, and 10 000 bending cycles (at a tensile strain of 0.3%) are presented in Figure 4f. The response characteristics of the device to IR are nearly unchanged, although there is a slight decrease in responsivity after more than 5000 bending cycles (see Figure 4f). From these results, it can be presumed that the sensing capability of the transparent, flexible R-GO/P(VDF-TrFE) nanocomposite FET after cyclic bending is relatively stable.

The transparent and flexible nanocomposite FET array with a R-GO concentration of 10 wt%, consisting of 4 × 4 devices, was fabricated to measure the distribution of IR radiation from the human body. We measured the normalized current ($(I_{DS} - I_{DS0})/I_{DS0}) \times 100\%$) of the 16 transparent and flexible nanocomposite FETs in the array under IR radiation from a human finger. **Figure 5** shows an example of the distribution of the $(I_{DS} - I_{DS0})/I_{DS0}) \times 100\%$ obtained from each device in the array. When the finger moves close to the half and quadrant devices (Figure 5a(1),a(2) and Figure 5b(1),b(2), respectively), we can see that there is a distribution of the $(I_{DS} - I_{DS0})/I_{DS0}) \times 100\%$ from the touched devices to the untouched devices, as shown in Figure 5a(3),b(3). The response current of the touched devices is higher than the devices near the touched region; devices which are farther from the touched regions show a lower response to IR radiation from the human body (Figure 5a(3),b(3)). Figure S11, Supporting Information, presents the distribution of the $(I_{DS} - I_{DS0})/I_{DS0}) \times 100\%$ under IR radiation from a human finger when the device is in a bent state. A tensile strain of 0.3% was applied to the device array and a finger was moved close to the entire and half devices (see Figure S11a(1),a(2) and Figure S11b(1),b(2), Supporting Information, respectively). In this case, to more clearly see the distribution of the drain current, we purposefully bent the device array so that the highest bending radius remained on the devices in column 3 (Figure S11a(2),b(2), Supporting Information). This means that when a finger was moved close to the entire and half of the device array (Figure S11a(1),a(2) and Figure S11b(1),b(2), Supporting Information), the devices in column 3 are directly in contact with the finger; therefore, the responsive current of the devices in column 3 is higher than the devices in the other columns (Figure S11a(3),b(3), Supporting Information). Measurement results of the IR detector array demonstrate the potential for applying our sensor array in human–electronics interfaces and in health monitoring devices.

3. Conclusions

In this paper, we demonstrated the IR detection capability of transparent and flexible nanocomposite R-GO/P(VDF-TrFE) FETs. The IR detector on the transparent and flexible substrate showed high transparency, flexibility, and stability under mechanical strain. The sensing mechanism of the device to IR is attributed primarily to the photon absorption and radiant heat absorption of the nanocomposite R-GO/P(VDF-TrFE) channel. When the R-GO/P(VDF-TrFE) nanocomposite thin film is exposed to IR, absorption of photons and heat of incident radiation produces electron–hole pairs and heat within the R-GO/P(VDF-TrFE) nanocomposite thin film. This produces a change in the conductance. In addition to IR absorption by R-GO in the R-GO/P(VDF-TrFE) nanocomposite channel, the absorption of incident IR can be enhanced by the additional IR absorbance of the polymer matrix, P(VDF-TrFE), as well as from the amount of R-GO inside the R-GO/P(VDF-TrFE) nanocomposite (which can be used to tune the IR absorption). Interestingly, the transparent and flexible nanocomposite FET is also highly responsive to IR radiation from the human body, so the distribution of IR radiation from a human finger was also

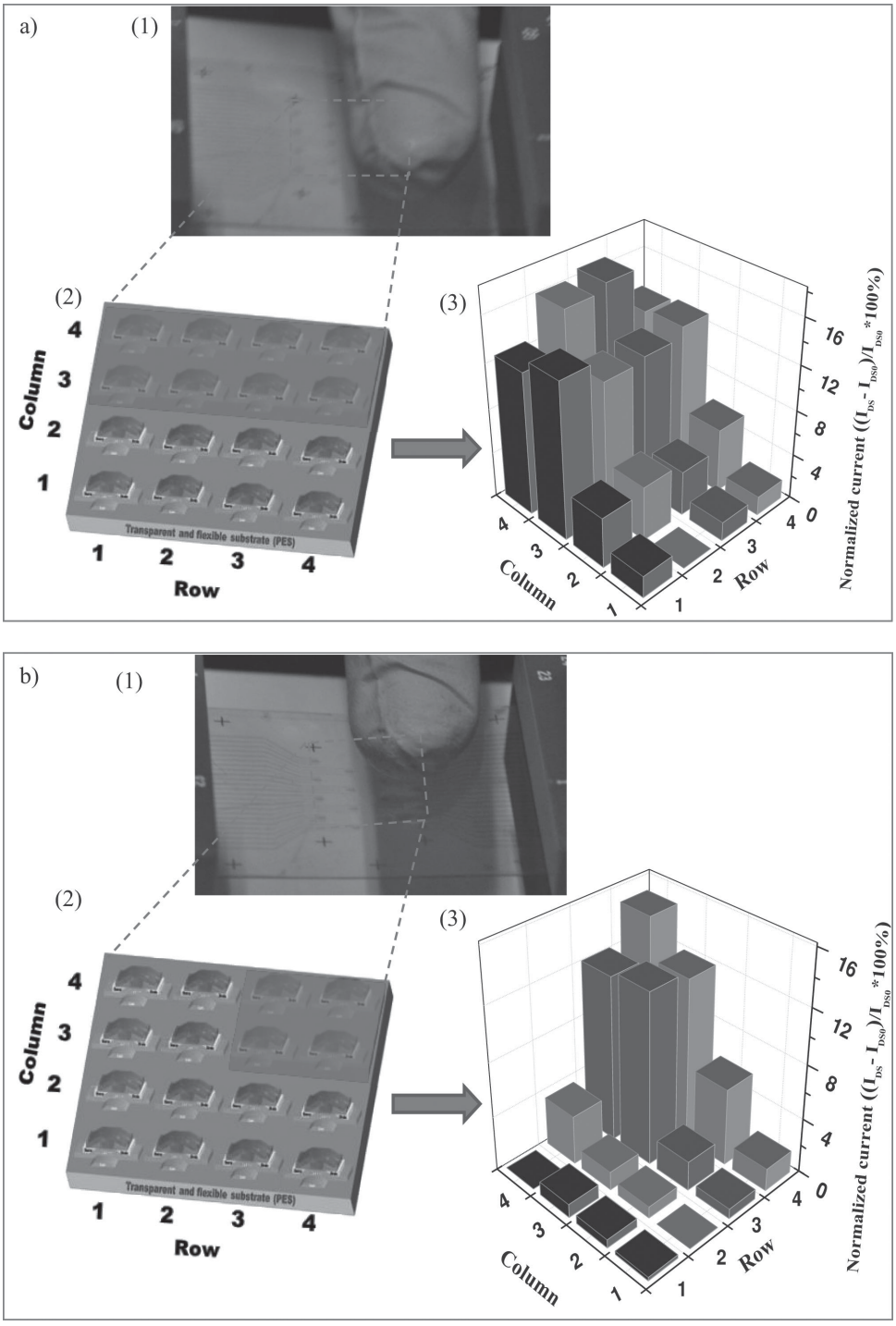

Figure 5. The distribution of the normalized current $((I_{DS} - I_{DS0})/I_{DS0} \times 100\%)$ obtained from each device in the array when a finger was moved close to the: a) half, and b) quadrant of the device array. The device at (column, row) = (1, 2) is defective. During monitoring of the I_{DS}, the V_G and V_{DS} were fixed at 9 and 10 V, respectively.

investigated. These results demonstrate that the transparent and flexible nanocomposite FET developed in this study, which is highly responsive to IR radiation from the human body, has great potential in a variety of applications including biomedical monitoring, IR imaging, and tactile sensing.

4. Experimental Section

Preparation of Functional Graphene Oxide: To facilitate the dispersion of graphene oxide (GO) in the polar aprotic solvent, *N*,*N*′-dimethylacetamide (DMAC), the carboxyl groups, and the hydroxyl groups were derivatized with amide and carbamate ester groups by

contacting graphite oxide with phenylisocyanate. GO nanosheets were prepared using a modified Hummer's method.[37] The derivatization of GO was performed using the procedure reported by Stankovich et al.[38] In brief, the saturated suspension of graphite oxide was prepared by stirring 500 mg of graphite oxide with 50 mL of *N*,*N*′-dimethylformamide (DMF) for 5 h. Then, 20×10^{-3} M (2.3826 g) of phenylisocyanate was added and stirred under a nitrogen atmosphere for 24 h. The reaction mixture was coagulated by being added into 500 mL of methylene chloride. The solvent was removed by filtration after precipitation. The precipitate was further washed two times with 500 mL of methylene chloride and dried overnight at ambient temperature to obtain graphite oxide with amide and carbamate esters. A functionalized GO nanosheet dispersion with a solid content of 5 mg was obtained by sonicating with phenylisocyanate-treated graphite oxide with DMAC.

Fabrication of R-GO/P(VDF-TrFE) Nanocomposite Thin Films: In this paper, the liquid phase blending method was used to prepare all R-GO/P(VDF-TrFE) nanocomposite thin films. P(VDF-TrFE) was dissolved in DMAC at a concentration 0.1 g mL^{-1}. GO nanosheets dispersed in DMAC at a concentration of 5 mg mL^{-1} were mixed with appropriate weight fractions of the P(VDF-TrFE) solution and stirred for 12 h before being sonicated for 10 min at room temperature. The GO nanosheets in the P(VDF-TrFE) matrix were reduced by a two-step in situ reduction technique, which consisted of a phenylhydrazine reduction (2 µL phenylhydrazine per 1 mL of dispersed GO in DMAC at a concentration 5 mg mL^{-1}) and a subsequent thermal reduction at 150 °C for 4 h under vacuum. To use the nanocomposite material as a channel layer in the FET, the R-GO/P(VDF-TrFE) nanocomposite thin film with 8 wt% loading of R-GO nanosheets was fabricated via spin-coating.

Fabrication of Transparent R-GO/P(VDF-TrFE) Nanocomposite FETs: Transparent R-GO/P(VDF-TrFE) nanocomposite FET devices were fabricated in a bottom-gate and bottom-contact configuration on both flexible and glass substrates. The spin-coated poly(3,4-ethylenedioxythiophene) poly(4-styrenesulfonate) (PEDOT:PSS), which was used as the gate, source, and drain electrodes, was patterned by an O_2 CDE (chemical dry etching) process. After spin-coating the PEDOT:PSS on both the poly(ether sulfones) (PES) (transparent and flexible device) and glass (transparent device) substrates, a thin film of Ni (5 nm) was deposited as an etch mask through a shadow mask onto the PEDOT:PSS film by e-beam evaporation. Then, the substrate was exposed to an oxygen microwave plasma in a CDE system at 640 mTorr. A microwave power of 500 W was used to etch the PEDOT:PSS that was unprotected by the Ni pattern. Finally, the Ni mask patterns were removed in an HNO_3 acid solution. With this patterning technique, transparent R-GO/P(VDF-TrFE) composite FETs with channel lengths ranging from 40 to 70 µm and a channel width of 800 µm were obtained. For the device on the glass substrate, a 200-nm-thick Al_2O_3 gate dielectric layer with low leakage current was deposited by ALD at 200 °C. Finally, an R-GO/P(VDF-TrFE) nanocomposite channel layer with an R-GO concentration of 8 wt% and a thickness of 200 nm was spin-coated on top of the source-drain electrodes. For the flexible device, a flexible gate dielectric is considered. And, for a gate dielectric with good mechanical property and low leakage current (gate dielectric showed low leakage current after cyclic bending from 100 to 10 000 cycles at strain 0f 0.3%) a hybrid organic-inorganic (Al_2O_3 (20 nm)/PVP (400 nm)/Al_2O_3 (20 nm)) gate dielectric layer was used. A 20-nm-thick Al_2O_3 layer was deposited by atomic layer deposition (ALD) at 200 °C, and a 400-nm-thick PVP was deposited via spin-coating.

Supporting Information

Supporting Information is available from the Wiley Online Library or from the author.

Acknowledgements

This research was supported by the Basic Science Research Program through the National Research Foundation (NRF) of Korea funded by the Ministry of Science, ICT & Future Planning (Grant No. 2013R1A2A1A01015232).

Received: December 26, 2014
Published online: February 11, 2015

[1] R.-H. Kim, D.-H. Kim, J. Xiao, B. H. Kim, S.-I. Park, B. Panilaitis, R. Ghaffari, J. Yao, M. Li, Z. Liu, V. Malyarchuk, D. G. Kim, A.-P. Le, R. G. Nuzzo, D. L. Kaplan, F. G. Omenetto, Y. Huang, Z. Kang, J. A. Rogers, *Nat. Mater.* **2010**, *9*, 929.
[2] X. Wang, W. Song, B. Liu, G. Chen, D. Chen, C. Zhou, G. Shen, *Adv. Funct. Mater.* **2013**, *23*, 1202.
[3] N. Liu, H. Tian, G. Schwartz, J. B.-H. Tok, T.-L. Ren, Z. Bao, *Nano Lett.* **2014**, *14*, 3702.
[4] S.-I. Park, Y. Xiong, R.-H. Kim, P. Elvikis, M. Meitl, D.-H. Kim, J. Wu, J. Yoon, C.-J. Yu, Z. Liu, Y. Huang, K.-C. Hwang, P. Ferreira, X. Li, K. Choquette, J. Rogers, *Science* **2009**, *325*, 977.
[5] R. V. Salvatierra, C. E. Cava, L. S. Roman, A. J. G. Zarbin, *Adv. Funct. Mater.* **2013**, *23*, 1490.
[6] Z. Goa, W. Jin, Y. Zhou, Y. Dai, B. Yu, Ch. Liu, W. Xu, Y. Li, H. Peng, Z. Liu, L. Dai, *Nanoscale* **2013**, *5*, 5576.
[7] W. Wang, M. Song, T.-S. Bae, Y. H. Park, Y.-C. Kang, S.-G. Lee, S.-Y. Kim, D. H. Kim, S. Lee, G. Min, G.-H. Lee, J.-W. Kang, J. Yun, *Adv. Funct. Mater.* **2014**, *24*, 1551.
[8] M. Kaltenbrunner, M. S. White, E. D. Głowacki, T. Sekitani, T. Someya, N. S. Sariciftci, S. Bauer, *Nat. Commun.* **2012**, *3*, 770.
[9] Z. Sun, Z. Liu, J. Li, G. Tai, S.-P. Lau, F. Yan, *Adv. Mater.* **2012**, *24*, 5878.
[10] G. Konstantatos, E. H. Sargent, *Nat. Nanotechnol.* **2010**, *5*, 391.
[11] A. M. Gobin, M. H. Lee, N. J. Halas, W. D. James, R. A. Drezek, J. L. West, *Nano Lett.* **2007**, *7*, 1929.
[12] J. Li, L. Niu, Z. Zheng, F. Yan, *Adv. Mater.* **2014**, *26*, 5239.
[13] A. J. Kreisler, A. Gaugue, *Supercond. Sci. Technol.* **2000**, *13*, 1235.
[14] A. Rogalski, J. Antoszewski, L. Faraone, *J. Appl. Phys.* **2009**, *105*, 091101.
[15] P. Avouris, *Nano Lett.* **2010**, *10*, 4285.
[16] F. Bonaccorso, Z. Sun, T. Hasan, A. C. Ferrari, *Nat. Photonics* **2012**, *4*, 611.
[17] Q. Bao, K. P. Loh, *ACS Nano* **2012**, *6*, 3677.
[18] W. Guo, S. Xu, Z. Wu, N. Wang, M. M. T. Loy, S. Du, *Small* **2013**, *9*, 3031.
[19] Y. Zhang, T. Liu, B. Meng, X. Li, G. Liang, X. Hu, Q. J. Wang, *Nat. Commun.* **2013**, *4*, 1811.
[20] M. C. Lemme, F. H. L. Koppens, A. L. Falk, M. S. Rudner, H. Park, L. S. Levitov, C. M. Marcus, *Nano Lett.* **2011**, *11*, 4134.
[21] C.-H. Liu, Y.-C. Chang, T. B. Norris, Z. Zhong, *Nat. Nanotechnol.* **2014**, *9*, 273.
[22] X. Wang, Z. Cheng, K. Xu, H. K. Tsang, J.-B. Xu, *Nat. Photonics* **2013**, *7*, 888.
[23] N. M. Gabor, J. C. W. Song, Q. Ma, N. L. Nair, T. Taychatanapat, K. Watanabe, T. Taniguchi, L. S. Levitov, P. Jarillo-Herrero, *Science* **2011**, *334*, 648.
[24] T. Mueller, F. Xia, P. Avouris, *Nat. Photonics* **2010**, *4*, 297.
[25] J. Park, *Nano Lett.* **2009**, *9*, 1742.
[26] F. Xia, T. Mueller, R. Golizadeh-Mojarad, M. Freitag, Y.-M. Lin, J. Tsang, V. Perebeinos, P. Avouris, *Nano Lett.* **2009**, *9*, 1039.
[27] F. Xia, T. Mueller, Y.-M. Lin, A. Valdes-Garcia, P. Avouris, *Nat. Nanotechnol.* **2009**, *4*, 839.
[28] R. S. Singh, V. Nalla, W. Chen, A. T. S. Wee, W. Ji, *ACS Nano* **2011**, *5*, 5969.
[29] M. Freitag, T. Low, F. Xia, P. Avouris, *Nat. Photonics* **2013**, *7*, 53.
[30] T. Q. Trung, N. T. Tien, D. Kim, J. H. Jung, O. J. Yoon, N.-E. Lee, *Adv. Mater.* **2012**, *24*, 5254.

[31] B. Chitara, L. S. Panchakarla, S. B. Krupanidhi, C. N. R. Rao, *Adv. Mater.* **2011**, *23*, 5419.
[32] H. Chang, Z. Sun, Q. Yuan, F. Ding, X. Tao, F. Yan, Z. Zheng, *Adv. Mater.* **2010**, *22*, 4872.
[33] Z. Liang, Z. Fu, S. Y. Chou, *Nano Lett.* **2007**, *7*, 3840.
[34] Q. He, H. G. Sudibya, Z. Yin, S. Wu, H. Li, F. Boey, W. Huang, P. Chen, H. Zhang, *ACS Nano* **2010**, *4*, 3201.
[35] Y. Guo, B. Wu, H. Liu, Y. Ma, Y. Yang, J. Zheng, G. Yu, Y. Liu, *Adv. Mater.* **2011**, *23*, 4626.
[36] T. Q. Trung, S. Ramasundaram, S. W. Hong, N.-E. Lee, *Adv. Funct. Mater.* **2014**, *24*, 3438.
[37] S. Park, J. An, I. Jung, R. D. Piner, S. J. An, X. Li, A. Velamakanni, R. S. Ruoff, *Nano Lett.* **2009**, *9*, 1593.
[38] S. Stankovich, R. D. Piner, S. B. T. Nguyen, R. S. Ruoff, *Carbon* **2006**, *44*, 3342.